

# Dynamic spin susceptibility of paramagnetic spinel $\text{LiV}_2\text{O}_4$

V. Yushankhai,<sup>1,2</sup> A. Yaresko,<sup>1</sup> P. Fulde,<sup>1</sup> and P. Thalmeier<sup>3</sup>

<sup>1</sup>*Max-Planck-Institut für Physik Komplexer Systeme, D-01187 Dresden, Germany*

<sup>2</sup>*Joint Institute for Nuclear Research, 141980 Dubna, Russia*

<sup>3</sup>*Max-Planck-Institut für Chemische Physik fester Stoffe, D-01187 Dresden, Germany*

(Dated: April 14, 2018)

## Abstract

In an attempt to explain inelastic neutron scattering data for  $\text{LiV}_2\text{O}_4$  the dynamical spin susceptibility  $\chi(\mathbf{Q}, \omega)$  at zero temperature is calculated. Starting point is a weak coupling approach based on the LDA bandstructure for that material. It is supplemented by a RPA treatment of local on-site interactions and contains an adjustable parameter. Due to the geometrically frustrated lattice structure the magnetic response is strongly enhanced in the vicinity of a nearly spherical surface in  $\mathbf{Q}$ -space. We compare these results with recent low-temperature neutron scattering data. The measured spin relaxation rate  $\Gamma$  is used to estimate the spin fluctuation contribution to the specific heat.

PACS numbers: 71.27.+a, 71.10.-w, 71.10.Fd, 71.30.+h

## I. INTRODUCTION

The metallic spinel  $\text{LiV}_2\text{O}_4$  has been identified as the first  $3d$  system with heavy quasiparticles.<sup>1,2,3</sup> The low temperature specific heat coefficient  $\gamma = C/T \simeq 0.4 \text{ J mol}^{-1}\text{K}^{-2}$  is considerably enhanced as compared with that of simple metals and the same holds true for the spin susceptibility  $\chi_S$ . For high temperatures,  $T > 50 \text{ K}$ , the latter shows a Curie-Weiss behavior,  $\chi_S(T) = \chi_0 + C/(T + \theta)$ , where the Curie constant  $C = 0.47 \text{ cm}^3\text{K}/(\text{mol V})$  and the Weiss temperature  $\theta = 63 \text{ K} > 0$  implies an antiferromagnetic interaction between the V ions. No magnetic ordering has been observed down to  $0.02 \text{ K}$ .<sup>1</sup> Concerning the entropy  $S(T)$  whose temperature dependence is determined from the specific heat, one finds that  $S(T = 60 \text{ K}) - S(0) \simeq 10 \text{ J}/(\text{mol}\cdot\text{K})$  which is close to  $2R\ln 2$  where  $R$  denotes the gas constant. Thus at  $60 \text{ K}$  there is nearly one excitation per V ion. This suggests strongly that the low-lying excitations which lead to the heavy quasiparticle behavior result from spin degrees of freedom. Needless to say that the original discovery of the heavy quasiparticles in  $\text{LiV}_2\text{O}_4$  has initiated many experimental studies to follow including transport, NMR,<sup>4,5</sup>  $\mu\text{SR}$ ,<sup>6</sup> PES,<sup>7</sup> and inelastic neutron scattering work.<sup>8,9,10</sup> A special feature of the spinels and hence of  $\text{LiV}_2\text{O}_4$  is that the V ions occupy the sites of a pyrochlore lattice. The latter consists of corner sharing tetrahedra. For a microscopic understanding of the observed heavy quasiparticle behavior with an average number  $n_d = 1.5$  of  $d$ -electrons per V ion, two different approaches starting from either a strong or a weak coupling limit are possible. They have been reviewed in Ref. [11] and we want to discuss them briefly now.

Density functional calculations based on the LDA demonstrate that electrons near the Fermi energy  $E_F$  are of  $t_{2g}$  character.<sup>12,13,14</sup> The calculated density of states within LDA is too small by a factor of 25 in order to explain the large  $\gamma$  coefficient. Therefore in Ref. [15] the limit of strong correlations was taken as a starting point. In that limit, charge fluctuations between V ions are strongly suppressed due to both the on-site and nearest neighbor inter-site electron Coulomb repulsions.<sup>16</sup> Thus, in the ground state slowly varying charge configurations include V sites that are either singly (spin-1/2) or doubly (spin-1) occupied. In the latter case  $S = 1$  is due to the Hund's rule. The ground state consists of configurations in which the spin-1/2 and spin-1 sites form two subsets of chains (rings) and the spin chains are effectively decoupled because of geometrical frustration in the pyrochlore lattice. Within this spin chain model, the nearest neighbor ( $nn$ ) exchange couplings  $J_{nn}$

are assumed only. The linear specific heat coefficient  $\gamma = 2k_B R/3J_{nn}$ , where  $k_B$  is the Boltzmann constant, of the spin-1/2 chains is found to be large. Only a factor of two is missing as compared with experiment. Here  $J_{nn} \simeq 3$  meV is the  $nn$  spin-1/2 chain coupling, as obtained from LDA+U calculations. The spin-1 chains with a gapped spectrum do not contribute to  $\gamma$  coefficient. Our recent analysis has shown, however, that in the model formulation the next-nearest ( $nnn$ ) coupling  $J_{nnn}$  cannot be excluded, which may lead to a considerable renormalization of the above estimate of  $\gamma$ . Moreover, if  $J_{nnn}/J_{nn} > 0.24$ , the spin-1/2 chain system may even enter the regime of dimerization. Of course, effects of the kinetic energy which were omitted so far should also be included in an extended spin chain model.

Because of these growing complications, it is of interest to investigate what results for the spin correlations are, when one starts from the limit of weak correlations instead. In this limit, the  $d$ -electrons are in broad LDA energy bands in contrast to nearly localized electronic states in the opposite limit. Since the effects of electron Coulomb repulsions are neglected (except for those already contained in the LDA), the geometrically frustrated lattice structure plays a role only as it affects the form of the LDA energy bands. As shown below, this results however in a characteristic form of the  $\mathbf{Q}$ -dependence of the unenhanced dynamic spin susceptibility  $\chi^{(0)}(\mathbf{Q}, \omega)$ . So the starting points of both approaches are very different. The hope is that both limits can eventually be brought to convergence in a region which is between the two limiting situations.

The present work was first motivated by results of quasielastic neutron scattering measurements<sup>8,9,10</sup> carried out on polycrystalline samples of  $\text{LiV}_2\text{O}_4$ . At low temperatures strong quasielastic neutron scattering was found in a range of wavevectors,  $0.4\text{\AA}^{-1} \lesssim Q \lesssim 0.8\text{\AA}^{-1}$ . The quasielastic linewidth  $\Gamma(Q)$  is of a few meV, indicating a slow spin dynamics in the above  $Q$  region. Because of the relation between the measured dynamic structure factor and the imaginary part of the dynamic spin susceptibility  $S(\mathbf{Q}, \omega; T) = (1 - e^{-\hbar\omega/k_B T}) \chi''(\mathbf{Q}, \omega; T)$ , calculation of  $\chi(\mathbf{Q}, \omega; T)$  is of fundamental importance to interpret inelastic neutron scattering data.

Our aim is to include a realistic electronic band structure for  $\text{LiV}_2\text{O}_4$  into RPA-like calculations of the dynamic spin susceptibility. The latter is enhanced due to exchange-correlation effects of electrons on the vanadium  $3d$ -orbitals. The calculations are performed for  $T=0$ . We restrict ourselves to the study of  $\chi(\mathbf{Q}, \omega)$  along high-symmetry directions

in the reciprocal space and focus on the analysis of its low frequency behavior. As shown below, even such a restricted consideration allows us to gain insight into the low-temperature spin dynamics of  $\text{LiV}_2\text{O}_4$  and provides a basis for a comparison of computational results with experimental data. Our main findings are the following (i) the dominant maxima of the calculated unenhanced spin susceptibility  $\chi^{(0)}(\mathbf{Q}, \omega)$ , i.e., the one from LDA occur in the same region of  $\mathbf{Q}$ -space where the largest intensity of the inelastic neutron scattering is found; (ii) a moderate value of the electronic local exchange-correlation coupling  $\mathcal{K}$  is sufficient within RPA to bring the system close to a magnetic instability and thus to a strong slowing down of spin fluctuations for wave vectors  $\mathbf{Q}$  determined by (i).

Because we assume local, Hubbard-like electron interactions, the exchange-correlation coupling  $\mathcal{K}$  is  $\mathbf{Q}$ -independent and therefore treated here as an orbital-independent adjustable parameter. Along the way, we will discuss possible extensions of the theory in some detail, but not pursue them further.

The random-phase approximation was applied to the one-band Hubbard model by Izuyama, Kim, and Kubo in their seminal work<sup>17</sup> and developed further by Doniach.<sup>18</sup> The multiband generalization of the RPA to the dynamic spin susceptibility adopted here is in a close relation with earlier works by Cook<sup>19</sup> and Callaway and co-workers.<sup>20,21</sup> We mention also papers by Stenzel and Winter<sup>22,23</sup> along that line. The connection with these works will be pointed out at various places in the discussion below.

We address also the problem of spin fluctuation contribution  $\gamma_{sf}$  to the low temperature specific heat coefficient  $\gamma$ . As known,<sup>24,25,26</sup> slow spin-fluctuation dynamics can be described approximately by a system of overdamped oscillators. In general, these oscillators are characterized by  $\mathbf{Q}$ -dependent spin relaxation rates  $\Gamma_{\mathbf{Q}}$ . Based on the available inelastic neutron scattering data<sup>8,9,10</sup> and our RPA calculation of  $\chi(\mathbf{Q}, \omega)$  in  $\text{LiV}_2\text{O}_4$ , we suggest below a model describing a particular distribution of  $\Gamma_{\mathbf{Q}}$  in  $\mathbf{Q}$ -space. Then we show that a diversity of experimentally determined values of  $\Gamma_{\mathbf{Q}}$  leads to a theoretical estimate for  $\gamma_{sf}$  that falls also into a broad range with the largest value being close to  $\gamma$  observed in experiment.

A similar RPA approach to a fluctuation mechanism in  $\text{LiV}_2\text{O}_4$  based on a tight binding model for the V-3d bands has been proposed in Ref. [27] in an attempt to explain the specific heat enhancement. The numerical calculations have been performed for the supersymmetric case where all spin/orbital fluctuations are controlled by the same nearly critical interaction parameter. In the numerical calculations the instability is obtained only around the center of

the Brillouin zone and the large mass enhancement is due to contributions from all possible spin/orbital fluctuations at  $\mathbf{Q}=0$ . In our approach we take the complementary view point that (i) only the spin fluctuations are close to be critical and (ii) the critical spin fluctuations at  $T = 0$  are located in a wide region of  $\mathbf{Q}$ -space far away from the Brillouin zone center in accord with the experimental evidence from inelastic neutron scattering. Thus in our model the extended region of nearly critical spin fluctuations in momentum space is a promising candidate for the large mass enhancement.

## II. ELECTRONIC BAND STRUCTURE AND UNENHANCED DYNAMIC SPIN SUSCEPTIBILITY OF $\text{LiV}_2\text{O}_4$

To define a reciprocal lattice for the cubic spinel structure of  $\text{LiV}_2\text{O}_4$ , it is convenient first to introduce the orthogonal basis vectors  $\mathbf{G}^{(\alpha)}$ , ( $\alpha = x, y, z$ ), of the length  $a^* = 2\pi/a \simeq 0.76\text{\AA}^{-1}$ ; here  $a=8.23\text{\AA}$  is the lattice parameter.<sup>3</sup> The irreducible Brillouin zone (BZ) of the underlying fcc lattice is a polyhedron depicted in Fig. 1, where X, Y, and Z points on their faces are given by the end points of the vectors  $\pm\mathbf{G}^{(\alpha)}$ . A cube that encloses the polyhedron provides us with a larger cubic BZ most appropriate to characterize periodic properties of  $\chi(\mathbf{Q}, \omega)$  in  $\mathbf{Q}$ -space. An arbitrary wavevector  $\mathbf{Q}$  will be denoted by  $\mathbf{Q} = \mathbf{q} + \mathbf{G}$ , where  $\mathbf{q}$  belongs to the first cubic BZ and  $\mathbf{G}$  is a reciprocal lattice vector;  $\mathbf{G} = 2 \sum_{\alpha} n_{\alpha} \mathbf{G}^{(\alpha)}$ , where  $n_{\alpha}$  are integer.

In the present work, the band structure for  $\text{LiV}_2\text{O}_4$  is calculated within the LDA in the framework of LMTO (linear muffin tin orbitals) and using the atomic sphere approximation. The main features of the calculated band structure agree well in many details with the LDA results obtained by other authors.<sup>12,13,14</sup>

In  $\text{LiV}_2\text{O}_4$  the vanadium  $3d$ -bands and the oxygen  $2p$ -bands are well separated by an energy  $\sim 2$  eV. The octahedral component of the crystal field is strong enough to split the vanadium  $3d$  bands into two separate and non-overlapping bands originating from  $t_{2g}$  and  $e_g$  orbitals. A weak trigonal component of the crystal field produces a further splitting of the low-lying set of  $t_{2g}$  orbitals into  $(a_{1g} + e'_g)$  orbitals. The latter dominate the electronic states near the vicinity of the Fermi energy. The complexity of the band structure results in many sheets of the Fermi surface.

Recalling that  $\text{LiV}_2\text{O}_4$  is found to be a paramagnet down to very low temperatures,

we assume that the system remains spin disordered at all temperatures, and carry out a calculation of the dynamic spin susceptibility for  $T = 0$ . Without external magnetic field the longitudinal and the transverse susceptibility are the same.

In the multi-band model under consideration, the time- and space-Fourier transform of the dynamic spin susceptibility for the LDA band electrons takes the familiar form

$$\chi_{\mathbf{G},\mathbf{G}'}^{(0)}(\mathbf{q},\omega) = \frac{1}{V} \sum_{\eta,\eta'} \sum_{\mathbf{k}} \gamma_{\eta'\eta}(\mathbf{k},\mathbf{q};\omega) \quad (1)$$

$$\times \langle \mathbf{k} - \mathbf{q}/2, \eta | e^{-i(\mathbf{q}+\mathbf{G})\mathbf{r}} | \mathbf{k} + \mathbf{q}/2, \eta' \rangle$$

$$\times \langle \mathbf{k} + \mathbf{q}/2, \eta' | e^{i(\mathbf{q}+\mathbf{G}')\mathbf{r}} | \mathbf{k} - \mathbf{q}/2, \eta \rangle,$$

$$\gamma_{\eta'\eta}(\mathbf{k},\mathbf{q};\omega) = -\frac{f_{\eta'}(\mathbf{k} + \mathbf{q}/2) - f_{\eta}(\mathbf{k} - \mathbf{q}/2)}{E_{\eta'}(\mathbf{k} + \mathbf{q}/2) - E_{\eta}(\mathbf{k} - \mathbf{q}/2) + \hbar\omega + i\delta}. \quad (2)$$

In (1) and (2), the plane-wave matrix elements are calculated on the basis of Bloch functions  $\psi_{\mathbf{k}\eta}(\mathbf{r})$  with the band index  $\eta$  and energy  $E_{\eta}(\mathbf{k})$ . Here  $f_{\eta}(\mathbf{k})$  is the Fermi distribution function.

In the next section, the exchange-correlation enhanced spin susceptibility  $\chi_{\mathbf{G},\mathbf{G}'}(\mathbf{q},\omega)$  is derived within the RPA. In this derivation,  $\mathbf{G} \neq \mathbf{G}'$  matrix elements of  $\chi_{\mathbf{G},\mathbf{G}'}^{(0)}(\mathbf{q},\omega)$  are involved, which lead to the well known problem of large matrix inversion. Since the magnetically active  $3d$ -orbitals of vanadium ions are rather compact, a large set of the reciprocal lattice vectors  $\mathbf{G}$  has to be taken into account and thus a matrix  $\chi_{\mathbf{G},\mathbf{G}'}^{(0)}(\mathbf{q},\omega)$  of high dimension has to be inverted. One encounters a similar problem when calculating the inverse dielectric matrix for electrons in transition metals.<sup>28</sup> To overcome this difficulty, an elegant procedure based on a simple and reliable approximation has been proposed and developed by several authors.<sup>21,28</sup> We are now in a position to discuss some preliminaries of this procedure, the central point of which is the search for a separable form for the plane-wave matrix elements entering Eq. (1).

Taking into account a four-site basis within the primitive lattice cell, there are altogether twelve bands of dominant  $d$ -character which originate from partially occupied  $a_{1g} + e'_g$  orbitals of the vanadium ions. Therefore, one expects that the Bloch functions  $\psi_{\mathbf{k}\eta}(\mathbf{r})$  for the actual  $d$ -bands near the Fermi energy can be well described by the orbital basis set  $\phi_{\mathbf{k},\tau m}$  of Bloch functions defined in terms of atomic-like  $a_{1g} + e'_g$ -orbitals localized on the pyrochlore lattice sites  $\mathbf{j} + \boldsymbol{\tau}$ :

$$\phi_{\mathbf{k},\tau m} = \frac{1}{\sqrt{N}} \sum_{\mathbf{j}} e^{i\mathbf{k}\mathbf{j}} w_m(\mathbf{r} - \mathbf{j} - \boldsymbol{\tau}). \quad (3)$$

Here the sum is over  $N$   $\mathbf{j}$ -sites of the underlying fcc lattice. The  $\boldsymbol{\tau}$ -vectors form a four-point basis. Furthermore,  $w_m(\mathbf{r} - \mathbf{j} - \boldsymbol{\tau})$  is the  $m$ -th orbital from the  $a_{1g} + e'_g$  orbital set on the pyrochlore lattice site  $\mathbf{j} + \boldsymbol{\tau}$ . For shortening the notation, we use below a composite index  $(\boldsymbol{\tau}m)$  to refer to  $w_m(\mathbf{r} - \mathbf{j} - \boldsymbol{\tau})$  as the  $(\boldsymbol{\tau}m)$ -th orbital belonging to the  $\mathbf{j}$ -th primitive lattice cell. We recall the following unitary transformation between the band and the orbital representations for Bloch functions

$$\psi_{\mathbf{k}\eta}(\mathbf{r}) = \sum_{\boldsymbol{\tau}m} a_{(\boldsymbol{\tau}m)\eta}(\mathbf{k}) \phi_{\mathbf{k},\boldsymbol{\tau}m}. \quad (4)$$

Here  $a_{(\boldsymbol{\tau}m)\eta}(\mathbf{k})$  are elements of the  $(12 \times 12)$ -matrix satisfying the following orthogonality and completeness relations

$$\begin{aligned} \sum_{\boldsymbol{\tau}m} a_{(\boldsymbol{\tau}m)\eta}^*(\mathbf{k}) a_{(\boldsymbol{\tau}m)\eta'}(\mathbf{k}) &= \delta_{\eta\eta'}, \\ \sum_{\eta} a_{(\boldsymbol{\tau}m)\eta}(\mathbf{k}) a_{(\boldsymbol{\tau}'m')\eta}^*(\mathbf{k}) &= \delta_{\boldsymbol{\tau}m, \boldsymbol{\tau}'m'}, \end{aligned} \quad (5)$$

where  $\delta$  is the Kronecker symbol. The plane-wave matrix elements in (1) can now be written as

$$\langle \mathbf{k} + \mathbf{q}/2, \eta' | e^{i(\mathbf{q} + \mathbf{G})\mathbf{r}} | \mathbf{k} - \mathbf{q}/2, \eta \rangle = \sum_{\boldsymbol{\tau}'m'} \sum_{\boldsymbol{\tau}m} A_{(\boldsymbol{\tau}'m')(\boldsymbol{\tau}m)}^{\eta'\eta}(\mathbf{k}, \mathbf{q}) \mathcal{F}_{(\boldsymbol{\tau}'m')(\boldsymbol{\tau}m)}(\mathbf{k}, \mathbf{q} + \mathbf{G}'), \quad (6)$$

where

$$A_{(\boldsymbol{\tau}'m')(\boldsymbol{\tau}m)}^{\eta'\eta}(\mathbf{k}, \mathbf{q}) = a_{(\boldsymbol{\tau}'m')\eta'}^*(\mathbf{k} + \mathbf{q}/2) a_{(\boldsymbol{\tau}m)\eta}(\mathbf{k} - \mathbf{q}/2), \quad (7)$$

while the form-factor  $\mathcal{F}$  involves integrals over pairs of  $w_m$ -orbitals localized either at the same site or at two different lattice sites. The compactness of these orbitals suggests to neglect the two-center integrals, which leads to the following approximation for the form factor

$$\begin{aligned} \mathcal{F}_{(\boldsymbol{\tau}'m')(\boldsymbol{\tau}m)}(\mathbf{k}, \mathbf{q} + \mathbf{G}) &\simeq \delta_{\boldsymbol{\tau}'\boldsymbol{\tau}} e^{i(\mathbf{q} + \mathbf{G})\boldsymbol{\tau}} \int d\mathbf{r} w_{m'}(\mathbf{r}) e^{i(\mathbf{q} + \mathbf{G})\mathbf{r}} w_m(\mathbf{r}) \\ &= \delta_{\boldsymbol{\tau}'\boldsymbol{\tau}} F_{(\boldsymbol{\tau}'m')(\boldsymbol{\tau}m)}(\mathbf{q} + \mathbf{G}). \end{aligned} \quad (8)$$

We have checked that the neglect of the overlap integrals between the calculated  $d$  orbitals on different sites in  $\text{LiV}_2\text{O}_4$  is a rather accurate approximation. The approximation results,

in particular, in a  $\mathbf{k}$ -independence of the form-factor  $F$  in (8), the advantage of which will be exploited in the next section. It is worth noting that in (8) the factors  $e^{i(\mathbf{q}+\mathbf{G})\boldsymbol{\tau}}$  are invariant under translations by  $2\mathbf{G}$  in reciprocal space.

For shortening the notation, it is helpful to replace in the upper equations the double ‘‘orbital’’ index  $(\boldsymbol{\tau}'m')(\boldsymbol{\tau}m)$  by a symbol  $L$  and to introduce the following orbitally projected expression

$$\begin{aligned} \gamma_{LL'}(\mathbf{q}, \omega) &= \frac{1}{N} \sum_{\eta, \eta'} \sum_{\mathbf{k}} \left[ A_L^{\eta'\eta}(\mathbf{k}, \mathbf{q}) \right]^* \\ &\quad \times \gamma_{\eta'\eta}(\mathbf{k}, \mathbf{q}; \omega) A_{L'}^{\eta'\eta}(\mathbf{k}, \mathbf{q}). \end{aligned} \quad (9)$$

In the following the left-hand side of Eq. (9) is referred to as the matrix  $\gamma$  in the orbital  $L$ -representation. The elements of the orbital  $\gamma$ -matrix are periodic in reciprocal space:  $\gamma_{LL'}(\mathbf{q} + \mathbf{G}, \omega) = \gamma_{LL'}(\mathbf{q}, \omega)$ . With these notations, the LDA spin susceptibility (1) takes the following form

$$\chi_{\mathbf{G}, \mathbf{G}'}^{(0)}(\mathbf{q}, \omega) = \sum_{LL'} F_L^*(\mathbf{q} + \mathbf{G}) \gamma_{LL'}(\mathbf{q}, \omega) F_{L'}(\mathbf{q} + \mathbf{G}'). \quad (10)$$

It is apparent from Eqs. (2), (9), and (10) that the computation of three types of quantities is required in a wide range of  $\mathbf{q}$ ,  $\mathbf{k}$ , and  $\omega$ : these are the multi-band matrix  $\gamma_{\eta'\eta}$ , the matrix elements  $A_L^{\eta'\eta}$  and the form factor  $F_L$ .

For an analysis of inelastic neutron scattering as a function of momentum  $\hbar(\mathbf{q} + \mathbf{G}) = \hbar\mathbf{Q}$  and energy  $\hbar\omega$  transfer, the diagonal ( $\mathbf{G}' = \mathbf{G}$ ) term  $\chi_{\mathbf{G}, \mathbf{G}}(\mathbf{q}, \omega) = \chi(\mathbf{Q}, \omega)$  should be calculated including the relevant electron interactions. This will be discussed in the next section. At this stage, we calculate first the unenhanced  $\chi^{(0)}(\mathbf{Q}, \omega)$ . This is done along three high-symmetry directions  $\Gamma\text{X}$ ,  $\Gamma\text{K}$  and  $\Gamma\text{L}$  in reciprocal space which are further abbreviated by X, K and L, respectively. For each of these directions D, wavevectors  $\mathbf{q}$  and  $\mathbf{G}$  are parallel and the use of a modulus  $Q^D$  of the wavevector  $\mathbf{Q} = \mathbf{q} + \mathbf{G}$  is sufficient, provided the system has space inversion symmetry.

In the static ( $\omega = 0$ ) limit, the spin susceptibility  $\chi^{(0)}(\mathbf{Q}, 0)$  is calculated and the results are displayed in Fig. 2 as a set of functions  $\chi_D^{(0)}(Q)$  with wavevectors of length  $Q$  along the directions  $D = \text{X, K, L}$ . For  $Q > 2a^*$  the susceptibility is considerably suppressed due to the form factor.

One notices a significant variation of  $\chi_D^{(0)}(Q)$  over the whole range of the wavevectors chosen. Since we intent to apply the RPA theory, the positions of the maxima in  $\mathbf{Q}$ -space of



the unenhanced susceptibility  $\chi^{(0)}(\mathbf{Q}, 0)$  provide a valuable information: at these wavevectors and in their vicinity one expects the strongest spin correlations when the enhanced  $\chi(\mathbf{Q}, 0)$  is calculated.

For each direction D, two maxima of  $\chi_D^{(0)}(Q)$  at wavevectors  $Q_{c1}^D$  and  $Q_{c2}^D$  are found; the second strongly suppressed maximum at  $Q_{c2}^L > 2a^*$  along the L-direction is not depicted here. The maxima at smaller  $Q_{c1}^D$  ( $< Q_{c2}^D$ ) are located in the first cubic BZ while those at  $Q_{c2}^D$  are in the next BZ.

From now on let us refer to the three wavevectors  $Q_c = Q_{c1}^{X,K,L}$  as the “critical” ones. From Fig. 2 we obtain the following estimates:  $Q_{c1}^X \approx 0.50\text{\AA}^{-1}$ ,  $Q_{c1}^K \approx 0.65\text{\AA}^{-1}$ , and  $Q_{c1}^L \approx 0.75\text{\AA}^{-1}$ . Remarkably, these three values occur within the range  $0.4\text{\AA}^{-1} \lesssim Q \lesssim 0.8\text{\AA}^{-1}$  where the main quasielastic neutron scattering is observed.<sup>8,9,10</sup>

The frequency distribution of spin fluctuations of the system of independent electrons may be seen from Fig. 3 where representative results of the calculated  $\text{Im}\chi_D^{(0)}(\mathbf{Q}, \omega)$  are shown for three wavevectors of different length chosen along each of the high-symmetry directions D. For instance, at small wavevectors  $Q$  along the L-direction,  $\text{Im}\chi_L^{(0)}(Q, \omega)$  shows a low- $\omega$  single-peaked structure. With increasing values of  $Q$ , the low- $\omega$  peak moves upward and an additional broad distribution arises and grows gradually at higher frequencies. At the “critical” wavevector  $Q_{c1}^L$ , the pronounced low- $\omega$  peak at  $\hbar\omega \sim 0.2$  eV still survives. However, a large portion of the spectral weight is found now within a broad distribution over much higher frequencies. As  $Q$  grows further, the low- $\omega$  peaked feature gets suppressed and most of the spectral weight is shifted to the high-frequency region. As long as considerable spectral weight of the low- $\omega$  peaked feature of  $\text{Im}\chi_L^{(0)}(Q, \omega)$  is present, like at  $Q \approx Q_{c1}^L$ , its position on the  $\omega$ -axis is regarded as a bare (unrenormalized) spin relaxation rate  $\Gamma^{(0)}(Q)$  characteristic of low- $\omega$  spin fluctuations. As expected, bare values of  $\Gamma^{(0)}(Q)$ , for instance,  $\Gamma^{(0)}(Q_{c1}^L) \approx 0.2$  eV, are much too high to explain the slow spin dynamics found in the experiment.<sup>8,9,10</sup> Similar arguments are also applicable to the behavior of  $\text{Im}\chi_D^{(0)}(Q, \omega)$  along K- and X-directions displayed in Fig. 3. Therefore interactions between quasiparticles must play an essential role to reach the observed energy scale  $\Gamma$  of spin fluctuations. In the next section, interaction effects are taken into account in the form of RPA theory.

### III. RPA APPROACH TO THE DYNAMIC SPIN SUSCEPTIBILITY OF $\text{LiV}_2\text{O}_4$

Within linear response theory, the time-Fourier transform of the dynamic spin susceptibility obeys the following integral equation

$$\begin{aligned} \chi(\mathbf{r}, \mathbf{r}'; \omega) &= \chi^{(0)}(\mathbf{r}, \mathbf{r}'; \omega) \\ &+ \int d\mathbf{r}'' \chi^{(0)}(\mathbf{r}, \mathbf{r}''; \omega) \mathcal{K}(\mathbf{r}'') \chi(\mathbf{r}'', \mathbf{r}'; \omega). \end{aligned} \quad (11)$$

Here  $\mathcal{K}(\mathbf{r})$  is a first derivative of the spin-dependent part of the exchange-correlation potential  $V_{xc}^s$  taken in the local approximation. Since  $\mathcal{K}(\mathbf{r})$  is a periodic function,  $\mathcal{K}(\mathbf{r} + \mathbf{j}) = \mathcal{K}(\mathbf{r})$ , its reciprocal-space counterpart  $\mathcal{K}(\mathbf{G})$  is a function of the reciprocal-lattice vectors  $\mathbf{G}$ . After performing the double space-Fourier transformation, Eq. (11) is expressed as

$$\begin{aligned} \chi_{\mathbf{G}\mathbf{G}'}(\mathbf{q}, \omega) &= \chi_{\mathbf{G}\mathbf{G}'}^{(0)}(\mathbf{q}, \omega) \\ &+ \sum_{\mathbf{G}_1\mathbf{G}'_1} \chi_{\mathbf{G}\mathbf{G}_1}^{(0)}(\mathbf{q}, \omega) \mathcal{K}_{\mathbf{G}_1\mathbf{G}'_1} \chi_{\mathbf{G}'_1\mathbf{G}'}(\mathbf{q}, \omega), \end{aligned} \quad (12)$$

with  $\mathcal{K}_{\mathbf{G}_1\mathbf{G}'_1} = \mathcal{K}(\mathbf{G}_1 - \mathbf{G}'_1)$ . Solving of Eq. (12) requires an inversion of an infinite matrix  $(1 - \chi^{(0)}\mathcal{K})_{\mathbf{G}\mathbf{G}'}$  in reciprocal-lattice ( $\mathbf{G}$ ) representation. To tackle the problem, first one has to examine the convergence of the matrix elements of the susceptibility as the dimension of the ( $\mathbf{G}$ )-basis increases. To avoid this we use below a procedure suggested and developed in Refs. [21,28].

The separable form (10) of  $\chi^{(0)} = F^*\gamma F$  allows us to solve the matrix inversion problem by transforming it from  $\mathbf{G}$ -representation to the orbital  $L$ -representation. Actually, the iteration procedure applied to Eq. (12) yields the matrix expansion  $\chi = F^*\gamma(1 + M + M^2 + \dots)F$ , where the matrix elements of  $M$  are

$$\begin{aligned} M_{L_1L_3}(\mathbf{q}, \omega) &= \sum_{L_2} \left[ \sum_{\mathbf{G}\mathbf{G}'} F_{L_1}(\mathbf{q} + \mathbf{G}) \mathcal{K}_{\mathbf{G}\mathbf{G}'} F_{L_2}^*(\mathbf{q} + \mathbf{G}') \right] \\ &\times \gamma_{L_2L_3}(\mathbf{q}, \omega). \end{aligned} \quad (13)$$

Assuming a convergence of the above power series of  $M$  at any  $\mathbf{q}$  and  $\omega$ , it can be converted into a familiar form  $[1 - M]^{-1}$ . Before doing this, let us consider the matrix elements  $[\sum F\mathcal{K}F^*]_{L_1L_2}$  entering the definition (13) of the matrix  $M$  and specify its indices as  $L_1 = (\boldsymbol{\tau}_1 m'_1)(\boldsymbol{\tau}_1 m_1)$  and  $L_2 = (\boldsymbol{\tau}_2 m'_2)(\boldsymbol{\tau}_2 m_2)$ . Then by using the definition (8) for the approximate form factor  $F$  and the inverse Fourier transformation for  $\mathcal{K}$ , a matrix element  $[\sum F\mathcal{K}F^*]_{L_1L_2}$

can be presented as a space integral of a product function of  $\mathcal{K}(\mathbf{r})$  and two pairs of localized orbitals  $w_m(\mathbf{r} - \mathbf{j} - \boldsymbol{\tau})$ . In general, there are one-center and two-center integrals. We neglect interactions between different sites and retain only the one-center integrals. Thus we use the approximation

$$\left[ \sum_{\mathbf{G}\mathbf{G}'} F(\mathbf{q} + \mathbf{G}) \mathcal{K}_{\mathbf{G}\mathbf{G}'} F^*(\mathbf{q} + \mathbf{G}') \right]_{L_1 L_2} \simeq \delta_{\boldsymbol{\tau}_1 \boldsymbol{\tau}_2} \mathcal{K}(m'_1 m_1; m'_2 m_2),$$

$$\mathcal{K}(m'_1 m_1; m'_2 m_2) = v_0 \int_{v_0} d\mathbf{r} w_{m'_1}(\mathbf{r}) w_{m_1}(\mathbf{r}) \mathcal{K}(\mathbf{r}) w_{m'_2}(\mathbf{r}) w_{m_2}(\mathbf{r}). \quad (14)$$

Furthermore, we neglect Hund's rule correlations and keep only the diagonal matrix elements  $\mathcal{K}(m, m; m, m)$ . Thus, the  $m$ -independent unique coupling constant  $\mathcal{K}$  is the only adjustable parameter in our approximate approach. Finally, we arrive at the following expression for the enhanced spin susceptibility

$$\chi_{\mathbf{G}, \mathbf{G}'}(\mathbf{q}, \omega) = \sum_{LL'L''} F_L^*(\mathbf{q} + \mathbf{G}) \gamma_{LL''}(\mathbf{q}, \omega) ([1 - \mathcal{K}\gamma(\mathbf{q}, \omega)]^{-1})_{L''L'} F_{L'}(\mathbf{q} + \mathbf{G}'), \quad (15)$$

where the elements of the matrix  $\gamma(\mathbf{q}, \omega)$  are given by (9). The essence of the procedure is instead of inverting the large matrix needed to solve the Eq. (12) to invert the smaller matrix  $(1 - \chi^{(0)}\mathcal{K})_{LL'}$  in the orbital basis.

Because of the composite character of orbital indices  $L$ , matrix operations in  $L$ -representation require additional comments. In particular, matrix elements of a transposed matrix  $\tilde{\gamma}$  are related to those of the direct matrix as  $\tilde{\gamma}_{L_1 L_2} = \gamma_{\bar{L}_2 \bar{L}_1}$ , where each composite index  $L_n = (\boldsymbol{\tau}'_n m'_n)(\boldsymbol{\tau}_n m_n)$  is also transposed to give  $\bar{L}_n = (\boldsymbol{\tau}_n m_n)(\boldsymbol{\tau}'_n m'_n)$ . Therefore, for a Hermitian conjugate matrix  $\gamma^\dagger$  one has  $\gamma^\dagger_{L_1 L_2} = \gamma^*_{\bar{L}_2 \bar{L}_1}$ . There are 144 distinct indices  $L$ , therefore  $\gamma$  is a (144×144)-matrix. The large number of elements  $\gamma_{LL'}(\mathbf{q}, \omega)$  that have to be determined for each value of  $\mathbf{q}$  and  $\omega$  makes the numerical calculations of  $\chi$  a rather complicated problem. At some stage pointed out below, we will introduce a simplification (“diagonal” approximation for the matrix  $\gamma$ ) allowing us to reduce the matrix dimensionality and, thus, make a numerical analysis feasible.

According to the definition (9), the matrix  $\gamma(\mathbf{q}, \omega)$  can be generally decomposed as follows

$$\gamma(\mathbf{q}, \omega) = \gamma^{(1)}(\mathbf{q}, \omega) + i\gamma^{(2)}(\mathbf{q}, \omega). \quad (16)$$

Here, the elements of the Hermitian matrix  $\gamma^{(1)} = (\gamma + \gamma^\dagger)/2$  are even functions of  $\omega$  while those of the anti-Hermitian matrix  $\gamma^{(2)} = (\gamma - \gamma^\dagger)/2i$  are odd functions of  $\omega$ . Note that  $\gamma^{(2)}(\mathbf{q}, 0) = 0$  for all  $\mathbf{q}$ .

Let us consider the static,  $\omega = 0$ , limit and solve the eigenvalue problem for the Hermitian matrix  $\gamma(\mathbf{q}, 0) = \gamma^{(1)}(\mathbf{q}, 0)$ :

$$\sum_{L'} \gamma_{LL'}(\mathbf{q}, 0) V_{L'}^{(k)}(\mathbf{q}) = \lambda^{(k)}(\mathbf{q}) V_L^{(k)}(\mathbf{q}), \quad (17)$$

where  $V_L^{(k)}$  are components of the  $k$ -th eigenvector with the eigenvalue  $\lambda^{(k)}$ . The static spin susceptibility takes the following form

$$\chi_{\mathbf{G}, \mathbf{G}'}(\mathbf{q}, 0) = \sum_k |\mathcal{F}^{(k)}(\mathbf{q}, \mathbf{G})|^2 \frac{\lambda^{(k)}(\mathbf{q})}{1 - \mathcal{K}\lambda^{(k)}(\mathbf{q})}, \quad (18)$$

with  $\mathcal{F}^{(k)}(\mathbf{q}, \mathbf{G}) = \sum_L F_L^*(\mathbf{q} + \mathbf{G}) V_L^{(k)}(\mathbf{q})$ . In solving Eq. (17), we adopt a “diagonal” approximation<sup>21</sup> which consists in retaining in  $\gamma_{LL'}$  only the diagonal composite indices,  $L = (\boldsymbol{\tau}m)(\boldsymbol{\tau}m)$  and  $L' = (\boldsymbol{\tau}'m')(\boldsymbol{\tau}'m')$ . Then  $\gamma_{LL'}$  becomes a (12×12)-matrix. A partial justification is that the moduli of the off-diagonal  $(\boldsymbol{\tau}'m') \neq (\boldsymbol{\tau}m)$ , matrix elements (7) are small in our calculations. To assess the accuracy of the “diagonal” approximation, a small set of arbitrary wavevectors  $\mathbf{q}$  was chosen and  $\text{Im}\chi^{(0)}(\mathbf{q}, \omega)$  was calculated (at  $\mathbf{G} = \mathbf{G}' = 0$ ) as a function of  $\omega$  including either all or only “diagonal” elements of the matrix  $\gamma$ . At each  $\mathbf{q}$  probed, we found rather tiny differences between the two curves.

Like in section II, we consider below only the high-symmetry X-, K- and L-directions in reciprocal space. For each direction D, let us pick out the “critical” wavevector  $Q_c^D$  and rearrange the set of  $\lambda^{(k)}(Q_c^D) = \lambda_D^{(k)}$  in the following order:  $\lambda_D^{(1)} > \lambda_D^{(2)} > \lambda_D^{(3)} > \dots$ . For brevity, a set of nondegenerate  $\lambda_D^{(k)}$  is discussed here. The first members of the set  $\lambda_D^{(k)}$  at  $k = 1, 2, \dots$  are positive in order to ensure  $\chi_{\mathbf{G}, \mathbf{G}'}(\mathbf{q}, 0) > 0$ , provided  $\mathcal{K}$  is below some critical value  $\mathcal{K}_c$ . It is apparent from (18) that along  $D$ -direction the  $\lambda_D^{(1)}$ -mode is the most “critical” one in the sense that  $0 \leq 1 - \mathcal{K}\lambda_D^{(1)} < 1 - \mathcal{K}\lambda_D^{(2)} < 1 - \mathcal{K}\lambda_D^{(3)} < \dots$ . A magnetic instability occurs if the condition  $1 - \mathcal{K}\lambda_D^{(1)} = 0$  is fulfilled. This defines  $\mathcal{K}_c$ . Among the three directions under consideration, the smallest  $\mathcal{K}_c = 0.49$  eV occurs along the L-direction at  $Q_{c1}^L \approx 0.75 \text{\AA}^{-1}$ . Since for X- and K-directions the instability conditions are fulfilled at values of  $\mathcal{K}$  that are close, but somewhat larger than  $\mathcal{K}_c = 0.49$  eV, the latter value is chosen to be the best estimate of the critical value of the exchange-correlation parameter

$\mathcal{K}$ . In  $\text{LiV}_2\text{O}_4$ , spin dynamics of a magnetically disordered state with strongly enhanced spin fluctuations may be described by Eq. (15) with the parameter  $\mathcal{K}$  approaching  $\mathcal{K}_c$  from below.

The enhancement of the static susceptibility (18) in a spin disordered state is controlled by a generalized Stoner factor  $S_{\mathcal{K}}(\mathbf{Q}) = [1 - \mathcal{K}\lambda^{(1)}(\mathbf{Q})]^{-1}$ , which is a function of both  $\mathcal{K}$  and  $\mathbf{Q}$ , with the obvious property  $S_{\mathcal{K}}(Q_{c1}^L) \rightarrow \infty$  as  $\mathcal{K} \rightarrow \mathcal{K}_c$ . Thus the Stoner factor describes the proximity of the system to the instability. As may be seen from Fig. 4, the strongest enhancement of the static susceptibility (18) is found for spin fluctuations at and nearby the “critical” wavevectors  $Q_c$  and at  $Q_{c2}^X$ . At the same time, the Stoner factor is of a moderate size for the remaining wavevectors.

Very similar  $Q$ -dependence of the exchange-correlation effects is seen from the calculated imaginary part of the enhanced dynamic spin susceptibility  $\text{Im}\chi_D(Q, \omega)$ .

Results for the calculated  $\text{Im}\chi_D(Q, \omega)$  are shown in Fig. 5. They have to be compared with the unenhanced spin susceptibility  $\text{Im}\chi_D^{(0)}(Q, \omega)$  plotted in Fig. 3. Let us follow the evolution of the  $\omega$ -dependence of  $\text{Im}\chi_L(Q, \omega)$  along the L-direction with increasing  $\mathcal{K} \rightarrow \mathcal{K}_c$ . Like in Fig. 3, three characteristic wavevectors are chosen to distinguish the behavior at “critical”  $Q^L \simeq Q_{c1}^L$  from those at smaller and larger wavevectors. As expected, the net frequency dependence of  $\text{Im}\chi_L(Q, \omega)$  is most strongly affected at  $Q_{c1}^L$ . In the upper panel of Fig. 5 a large portion of the spectral weight is transferred to the low energy region though at  $Q_{c1}^L$  the overall spectral distribution still extends up to  $\sim 2$  eV. The pronounced low- $\omega$  feature seen at  $Q_{c1}^L$  strongly dominates those at smaller and larger wavevectors.

Generally, in the low- $\omega$  limit the imaginary part of  $\chi(Q, \omega)$  can be accurately approximated by

$$\text{Im}\chi(Q, \omega) \simeq z_Q \chi(Q) \omega / \Gamma(Q), \quad (19)$$

where the weight factor  $z_Q < 1$ . Again, by choosing the L-direction as the most representative one, we have compared the initial gradients of several curves representing  $\text{Im}\chi_L(Q_{c1}, \omega)$  for different  $\mathcal{K} \lesssim \mathcal{K}_c$ , and found that the initial slope is proportional to  $S_{\mathcal{K}}^2(Q_{c1}^L)$  and thus grows very fast as  $\mathcal{K} \rightarrow \mathcal{K}_c$ . The factor  $S_{\mathcal{K}}^2(Q)$  stems from the Stoner enhanced static susceptibility,  $\chi(Q) \simeq S_{\mathcal{K}}(Q)\chi^{(0)}(Q)$ , and a renormalization of the spin relaxation rate,  $\Gamma(Q) \simeq \Gamma^{(0)}(Q)/S_{\mathcal{K}}(Q)$ . Far away from  $Q_{c1}^L$  the same relation holds, however, with much weaker enhancement factor,  $S_{\mathcal{K}}^2(Q^L) \ll S_{\mathcal{K}}^2(Q_{c1}^L)$ . Concerning the evolution of  $\text{Im}\chi_D(Q, \omega)$  for  $D = X, K$  with increasing  $\mathcal{K}$ , our calculations show a similar behavior, i.e., strongly

enhanced spin fluctuations at  $Q^D \sim Q_c^D$  in the low- $\omega$  region.

If the value of the adjustable coupling parameter  $\mathcal{K}$  is tuned close to  $\mathcal{K}_c$  then  $\Gamma(Q_c)$  may be reduced to values as low as the experimentally observed ones. However, this should not be taken as a literal explanation of experimental data because close to the critical condition RPA becomes unreliable. Furthermore, in our approach we ignored the quantitative contribution of inter-site charge fluctuations to the reduction of  $\Gamma^{(0)}$ . Instead, our purpose is to show that like in many other materials, in the case of  $\text{LiV}_2\text{O}_4$  the RPA theory is a useful tool to take into account the qualitative effects of strong electron correlations which provide a basic mechanism for a strong reduction of spin relaxation rate in a broad region of  $\mathbf{Q}$ -space.

#### IV. DISCUSSION

In this section we want to put our results in a more general context.

Quasielastic neutron scattering studies of powder samples of  $\text{LiV}_2\text{O}_4$  suggest that in the low- $T$  limit and in a range of wavevectors  $0.4\text{\AA}^{-1} \lesssim Q \lesssim 0.8\text{\AA}^{-1}$  the vanadium spin system exhibits strongly enhanced and slow spin fluctuations. A complete theoretical analysis of these data would require calculations of the dynamic spin susceptibility in a wide range of  $(\mathbf{Q}, \omega)$ -space. In principle, that is possible within our approximation scheme except for the large computational time required. The calculation of  $\chi(\mathbf{Q}, \omega)$  can be performed in any domain of  $(\mathbf{Q}, \omega)$ -space, not only along the high-symmetry  $\mathbf{Q}$ -directions. However, even the limited results of sections II and III provide a valuable and essential piece of information on the spin fluctuation dynamics in  $\text{LiV}_2\text{O}_4$ .

Actually, a particular  $\mathbf{Q}$ -dependence of the calculated unenhanced spin susceptibility  $\chi^{(0)}(\mathbf{Q}, 0)$  which involves the actual band structure of  $\text{LiV}_2\text{O}_4$ , clearly displays in Fig. 2 that the particular, “critical”, wavevectors  $Q_{c1}^{X,K,L}$  are grouped in the range  $0.5\text{\AA}^{-1} \lesssim Q_c \lesssim 0.8\text{\AA}^{-1}$  where the pronounced quasielastic neutron scattering is observed. However, the bare spin relaxation rate  $\Gamma^{(0)}(Q) \sim 200$  meV is much too large to be compatible with experimental observations. This disagreement has to be attributed to strong electron correlations not included in LDA calculations. Taking them into account by means of a RPA we have obtained an enhanced susceptibility  $\chi(\mathbf{Q}, \omega)$  as is seen by comparing Figs. 3 and 5. As the coupling tends to the critical value,  $\mathcal{K} \rightarrow \mathcal{K}_c$ , spin fluctuations near  $Q_c$  are strongly renormalized: a large fraction of the spectral weight is shifted to low frequencies, thus

resulting in an enhanced low-energy response.

Next we want to discuss in more detail the part of  $\mathbf{Q}$ -space with slow spin fluctuations. The wavevectors  $\mathbf{Q}_c = \mathbf{Q}_{c1}^{X,K,Z}$  are positioned on a smooth three dimensional surface to which we refer as “critical”  $\mathbf{q}_c$ -surface. This surface is in the first cubic Brillouin zone and we shall replace  $\mathbf{Q}$  by  $\mathbf{q}$  in that case. We have checked by additional calculations that spin fluctuations are slow everywhere on the  $\mathbf{q}_c$ -surface. Moreover, the broad maxima of  $\chi(\mathbf{q}, 0)$  in Fig. 4 suggest that the region of slow fluctuations extends over a width of  $(|\mathbf{q}_c| - \delta q/2) < |\mathbf{q}| < (|\mathbf{q}_c| + \delta q/2)$ , while the  $\mathbf{q}_c$ -surface lies midway between two bounds. The lower bound of this region is shown by the surface depicted in Fig. 6. It intersects the X-axis (and the equivalent Y- and Z-axes) at  $(q_{c1}^X - \delta q/2) \approx 0.5a^* \approx 0.4\text{\AA}^{-1} \equiv q_1^X$ . The upper bound is a congruent surface crossing the X-axis at  $(q_{c1}^X + \delta q/2) \approx 0.8a^* \approx 0.6\text{\AA}^{-1} \equiv q_2^X$ . Thus  $q_1^X$  and  $q_2^X$  are minimal radii of two bounds. The width  $\delta q$  is estimated to be  $\delta q \approx 0.3a^* \lesssim 0.23\text{\AA}^{-1}$ . Multiplicity of “critical” wavevectors distributed over an extended region in  $\mathbf{q}$ -space is a consequence of geometrical frustration in the pyrochlore lattice.

The suggested distribution in  $\mathbf{q}$ -space of strongly enhanced and slow spin fluctuations is compatible with the angular averaged data derived from inelastic neutron scattering on polycrystalline samples.<sup>8,9,10</sup> Indeed, as seen from Fig. 4, the next pronounced maximum of  $\chi(\mathbf{Q}, 0)$  is found along the X-direction at  $Q_{c2}^X \approx 1.4a^* \approx 1\text{\AA}^{-1}$ . Together with the other equivalent directions, it makes up a 6-point manifold but their partners at  $Q_{c2}^{K,L}$  are strongly suppressed by the form-factor. Therefore, this secondary manifold is not resolved in the experiment.

Many metallic systems with enhanced spin fluctuations show dramatically renormalized thermodynamic properties, for instance, a tendency to the formation of heavy-fermion properties: a strongly enhanced linear term  $\gamma T$  of the specific heat and a concomitantly enhanced magnetic susceptibility  $\chi$ . In many  $4f$ - and  $5f$ -derived heavy-fermion system the spin fluctuations are soft (have low  $\omega$ ) over large portion of the reciprocal space, which provides a large value of  $\gamma$ . A different case is the nearly antiferromagnetic metal  $\text{Cr}_{0.95}\text{V}_{0.05}$  which is close to incommensurate magnetic order. In contrast to the heavy-fermion systems,  $\text{Cr}_{0.95}\text{V}_{0.05}$  has a typical, unenhanced value of the measured  $\gamma$  which is explained<sup>29</sup> to be due to the small region in the momentum space occupied by the exchange enhanced soft spin fluctuations in this material.

It is promising now to develop a spin fluctuation theory for  $\text{LiV}_2\text{O}_4$  and estimate the

contribution of spin fluctuations to the low- $T$  specific heat. The theory is aimed at an approximate description of the low- $\omega$  behavior of the calculated  $\chi(\mathbf{q}, \omega)$  in terms of overdamped oscillators. One has to start with the following definition of the spin fluctuation free energy<sup>24,25,26</sup>

$$F_{sf} = \frac{3}{\pi} \sum_{\mathbf{q}} \int_0^{\omega_c} d\omega F_{osc}(\omega) \frac{z(\mathbf{q})\Gamma(\mathbf{q})}{\omega^2 + \Gamma^2(\mathbf{q})}, \quad (20)$$

where  $F_{osc}(\omega) = k_B T \ln[1 - \exp(-\hbar\omega/k_B T)]$  is the thermal part of the free energy of an oscillator;  $z(\mathbf{q})$  is the spectral weight of a low- $\omega$  spin fluctuation mode and  $\omega_c$  is the cutoff frequency. The specific heat is given by  $C_{sf}(T) = -T/N(\partial^2 F_{sf}/\partial T^2)$ , where  $N$  is the number of V-atoms in the system. In the limit  $T \rightarrow 0$ , simple calculation leads to the familiar expression for the spin fluctuation contribution  $\gamma_{sf} = C_{sf}(T)/T$  to the specific heat coefficient  $\gamma$ :

$$\gamma_{sf} = \frac{k_B^2 \pi}{N} \sum_{\mathbf{q}} \frac{z(\mathbf{q})}{\hbar\Gamma(\mathbf{q})}, \quad (21)$$

where the summation is over the cubic BZ.

Our aim now is to propose a reliable simple model describing variations of  $z(\mathbf{q})$  and  $\Gamma(\mathbf{q})$  in  $\mathbf{q}$ -space. The model adopts the most essential low- $\omega$  properties of  $\chi(\mathbf{q}, \omega)$  calculated for  $\text{LiV}_2\text{O}_4$ . We start by partitioning the  $\mathbf{q}$ -space into three regions: (I) the interior of the surface depicted in Fig. 6, i.e.,  $|\mathbf{q}| < (|\mathbf{q}_c| - \delta q/2)$ , (II) the ‘‘critical’’ region  $(|\mathbf{q}_c| - \delta q/2) < |\mathbf{q}| < (|\mathbf{q}_c| + \delta q/2)$ , and (III) the periphery,  $|\mathbf{q}| > (|\mathbf{q}_c| + \delta q/2)$ , of the cubic BZ. Within the layer (II) we approximate  $\Gamma(\mathbf{q})$  and  $z(\mathbf{q})$  by constants,  $\Gamma$  and  $z_{II} < 1$ , respectively. Then, in the region (I)  $\Gamma_I(\mathbf{q}) = (q/q_1)\Gamma$  and  $z_I(\mathbf{q}) = 1 - (1 - z_{II})q/q_1$ , which provides a piecewise continuity between regions (I) and (II). Here  $q_1 \simeq 0.5a^*$  and  $q_2 \simeq 0.8a^*$  are minimal radii of the lower (Fig. 6) and the upper bound surfaces for the ‘‘critical’’ region. Finally, as suggested from the analysis of  $\text{Im}\chi(\mathbf{q}, \omega)$  at large  $\mathbf{q}$ , in (III) the weight  $z(\mathbf{q})$  decreases fast to zero. Therefore, this contribution is neglected below. After performing the integration in (21) we arrive at the following expression

$$\gamma_{sf} = \frac{\pi^2}{32} k_B^2 \left[ \left(\frac{q_1}{a^*}\right)^3 + 2z_{II} \left(\frac{q_2}{a^*}\right)^3 \right] \frac{1}{\hbar\Gamma}. \quad (22)$$

Factor 3/2 involved in Eq. (22) takes into account a deviation of the ‘‘critical’’ surface shape from a spherical one.

An analysis of the calculated  $\text{Im}\chi(\mathbf{q}, \omega)$  leads us to a rather rough estimate  $z_{II} \approx 1/4$ , while the reported<sup>8,9,10</sup> low- $T$  values of  $\hbar\Gamma$  in the ‘‘critical’’ region of  $\mathbf{q}$  fall within the limits



of  $0.5\text{meV} < \hbar\Gamma < 5\text{meV}$ . By substituting these parameters into (22) and recalling that there are two V-atoms in the formula unit, we obtain the estimate for  $\gamma_{sf}$  as  $300 > \gamma_{sf} > 30$  in units of  $\text{mJ}/\text{K}^2\text{mol}$ . This estimate shows that slow spin fluctuations over an extended region in  $\mathbf{q}$ -space may explain the size of the enhanced specific heat coefficient in  $\text{LiV}_2\text{O}_4$ .

It is instructive to estimate the Sommerfeld-Wilson ratio  $R_W = \pi^2 k_B^2 \chi_S(T=0)/(3\mu_B^2 \gamma)$ , where  $\mu_B$  is Bohr magneton. Taking the upper bound for  $\gamma$  coefficient as  $\gamma \simeq 300 \text{ mJ}/\text{K}^2\text{mol}$  and the value  $\chi_S(T=0) = \chi(0,0)$  calculated for  $\mathcal{K} = 0.95\mathcal{K}_c$  in our theory, one obtains  $R_W \approx 5$ . This result is in a contrast with the estimate  $R_W \sim 0.1$  obtained within the RPA theory<sup>27</sup> where both spin and orbital critical fluctuations were assumed to contribute.

## V. CONCLUSIONS

The enhanced dynamic spin susceptibility of the multi-band paramagnetic spinel  $\text{LiV}_2\text{O}_4$  was calculated on the basis of the actual LDA band structure of this metallic system. It was shown that the complexity of the band structure results in an unenhanced spin susceptibility that displays a key information about spin fluctuations in this material, namely, the position in  $\mathbf{Q}$ -space of dominant spin correlations. The calculated moduli of these ‘‘critical’’ wave-vectors  $\mathbf{Q}_c$  located (at  $T=0$ ) obviously far away from the Brillouin zone center are in a good agreement with experiment.

The susceptibility enhancement due to electron interaction is described and calculated in the RPA approach adopted to the actual multi-band system with nearly degenerate  $d$ -orbitals. The most substantial approximation we made is the neglect of the orbital dependence and the off-diagonal matrix elements of the matrix  $\mathcal{K}$  defined by Eq. (14). A wave-vector dependence of  $\mathcal{K}$  is also omitted, which, we believe, is less crucial since the vanadium  $d$ -orbitals are well localized and strong on-site electronic correlations dominate. The approach developed above may be extended in the following ways. Provided a particular model of electron interaction is chosen and parameterized suitably, matrix elements of the  $\mathcal{K}$  matrix entering the expression (15) may be evaluated.<sup>30</sup> The resulting few-parameter theory then can be put on a quantitative ground by comparing the calculated model results with available experimental data.

Despite the approximations used in the description of electron correlations in a multi-band electronic system like  $\text{LiV}_2\text{O}_4$ , we believe that the approach developed here enabled us

to catch, in accord with experimental observations, the most essential effect of correlations: enormous magnification and slowing down of spin fluctuations at “critical” wave vectors  $\mathbf{Q}_c$ .

To our opinion, the obtained value of the critical coupling constant  $\mathcal{K}_c=0.49$  eV, at which a magnetic instability may occur in  $\text{LiV}_2\text{O}_4$ , is rather low, which means that a generalized Stoner criterion can be easily fulfilled. This finding is in agreement with the discussion in Refs. [13,14]. There, the authors performed spin-polarized LDA band structure calculations and noted a close proximity of the paramagnetic  $\text{LiV}_2\text{O}_4$  to different types of magnetic instabilities.

### Acknowledgments

One of the authors, V.Yu., acknowledges support from Deutsche Forschungsgemeinschaft under SFB 463.

- 
- <sup>1</sup> S. Kondo, D. Johnston, C. Swenson, F. Borsa, A. Mahajan, L. Miller, T. Gu, A. Goldman, M. Maple, D. Gajewski, et al., *Phys. Rev. Lett.* **78**, 3729 (1997).
  - <sup>2</sup> D. Johnston, *Physica B* **281–282**, 21 (2000).
  - <sup>3</sup> S. Kondo, D. C. Johnston, and L. L. Miller, *Phys. Rev. B* **59**, 2609 (1999).
  - <sup>4</sup> N. Fujiwara, H. Yasuoka, and Y. Ueda, *Phys. Rev. B* **57**, 3539 (1998).
  - <sup>5</sup> K. Fujiwara, K. Miyoshi, J. Takeuchi, Y. Shimaoka, and T. Kobayashi, *J. Phys. Condens. Matter* **16**, S615 (2004).
  - <sup>6</sup> A. Koda, R. Kadono, K. Ohishi, S. Saba, W. Higemoto, Y. Matsushita, and Y. Ueda, *J. Phys. Condens. Matter* **17**, L257 (2005).
  - <sup>7</sup> A. Shimoyamada, S. Tsuda, K. Ishizaka, T. Kiss, T. Shimojima, T. Togashi, S. Watanabe, C. Q. Zhang, C. T. Chen, Y. Matsushita, et al., *Phys. Rev. Lett.* **96**, 026403 (2006).
  - <sup>8</sup> A. Krimmel, A. Loidl, M. Klemm, S. Horn, and H. Schober, *Phys. Rev. Lett.* **82**, 2919 (1999).
  - <sup>9</sup> S. H. Lee, Y. Qiu, C. Broholm, Y. Ueda, and J. J. Rush, *Phys. Rev. Lett.* **86**, 5554 (2001).
  - <sup>10</sup> A. Murani, A. Krimmel, J. Stewart, M. Smith, P. Strobel, A. Loidl, and A. Ibarra-Palos, *J. Phys. Condens. Matter* **16**, S607 (2004).
  - <sup>11</sup> P. Fulde, *J. Phys. Condens. Matter* **16**, S591 (2004).

- <sup>12</sup> J. Matsuno, A. Fujimori, and L. F. Mattheiss, Phys. Rev. B **60**, 1607 (1999).
- <sup>13</sup> D. J. Singh, P. Blaha, K. Schwarz, and I. I. Mazin, Phys. Rev. B **60**, 16359 (1999).
- <sup>14</sup> V. Eyert, K.-H. Höck, S. Horn, A. Loidl, and P. S. Riseborough, Europhys. Lett. **46**, 762 (1999).
- <sup>15</sup> P. Fulde, A. Yaresko, A. Zvyagin, and Y. Grin, Europhys. Lett. **54**, 779 (2001).
- <sup>16</sup> V. Yushankhai, P. Fulde, and P. Thalmeier, Phys. Rev. B **71**, 245108 (2005).
- <sup>17</sup> T. Izuyama, D. Kim, and R. Kubo, J. Phys. Soc. Jpn. **18**, 1025 (1963).
- <sup>18</sup> S. Doniach, Proc. Phys. Soc. London **91**, 86 (1967).
- <sup>19</sup> J. Cooke, Phys. Rev. B **7**, 1108 (1973).
- <sup>20</sup> J. Callaway and C. Wang, J. Phys. F **5**, 2119 (1975).
- <sup>21</sup> J. Callaway, A. K. Chatterjee, S. P. Singhal, and A. Ziegler, Phys. Rev. B **28**, 3818 (1983).
- <sup>22</sup> E. Stenzel and H. Winter, J. Phys. F **15**, 1571 (1985).
- <sup>23</sup> E. Stenzel and H. Winter, J. Phys. F **16**, 1789 (1986).
- <sup>24</sup> G. Lonzarich, J. Magn. Magn. Mater **54–57**, 612 (1986).
- <sup>25</sup> G. Lonzarich, N. Bernhoeft, and D. Paul, Physica B **156**, 699 (1989).
- <sup>26</sup> R. Konno and T. Moriya, J. Phys. Soc. Jpn. **56**, 3270 (1987).
- <sup>27</sup> Y. Yamashita and K. Ueda, Phys. Rev. B **67**, 195107 (2003).
- <sup>28</sup> W. Hanke, Phys. Rev. B **8**, 4585 (1973).
- <sup>29</sup> S. M. Hayden, R. Double, G. Aeppli, T. G. Perring, and E. Fawcett, Phys. Rev. Lett. **84**, 999 (2000).
- <sup>30</sup> J. M. Bass, J. A. Blackman, and J. F. Cooke, Phys. Rev. B **53**, 2556 (1996).

## Figures

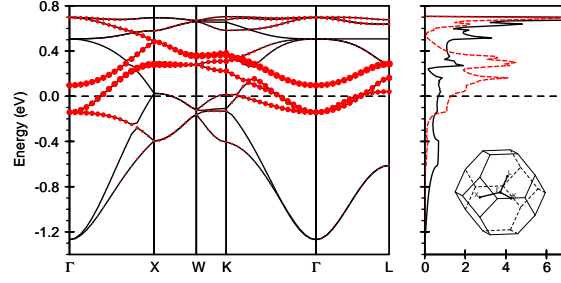


FIG. 1: (Color online) LDA bands originating from V  $d a_{1g}$  and  $e'_g$  states (left panel) and orbital resolved densities of states per eV, per V-atom (right panel). Densities of  $a_{1g}$  and  $e'_g$  states are plotted by dashed and solid lines, respectively. The size of circles in the left panel is proportional to the weight of the  $a_{1g}$  orbital in the state. The Fermi energy is at zero.

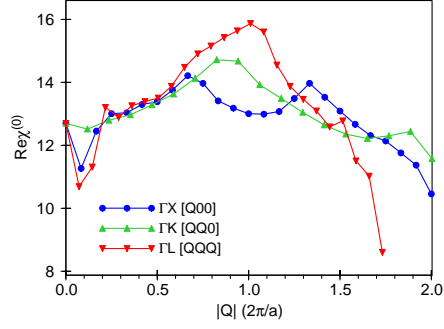


FIG. 2: (Color online) Unenhanced static spin susceptibility  $\chi^{(0)}(\mathbf{Q}, 0)$ , in states per eV, per primitive cell (4 V-atoms), calculated along high symmetry directions as a function of  $|\mathbf{Q}|$ .

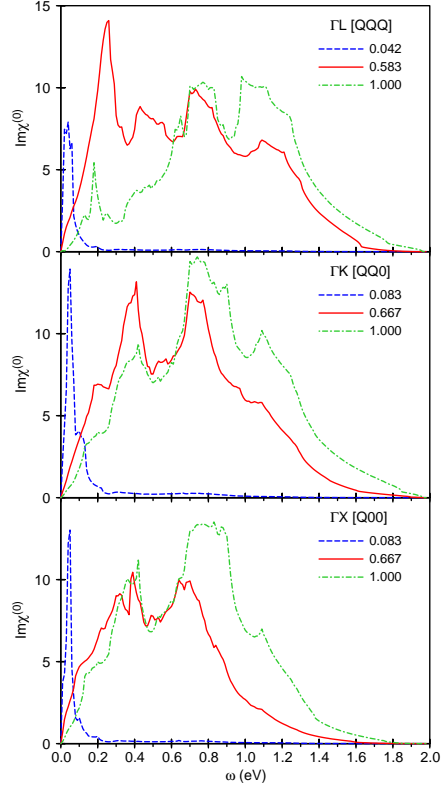


FIG. 3: (Color online) Unenhanced  $\text{Im}\chi^{(0)}(\mathbf{Q}, \omega)$  calculated at three different wave-vectors chosen along the high symmetry directions  $D=L, K, X$ . The “critical” wave-vectors  $Q_{c1}^{L,K,X}$  are denoted by the Cartesian component lengths: 0.583; 0.667; 0.667 (in units  $a^*$ ), respectively.

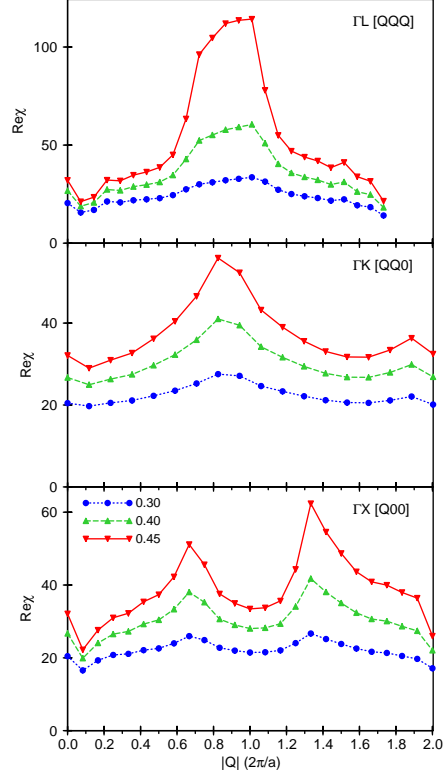


FIG. 4: (Color online) Evolution of the static spin susceptibility  $\chi(\mathbf{Q}, 0)$  for different values of the coupling constant  $\mathcal{K} \rightarrow \mathcal{K}_c = 0.49\text{eV}$ . Representative values of  $\mathcal{K}$  (in eV) chosen are shown in the low panel.



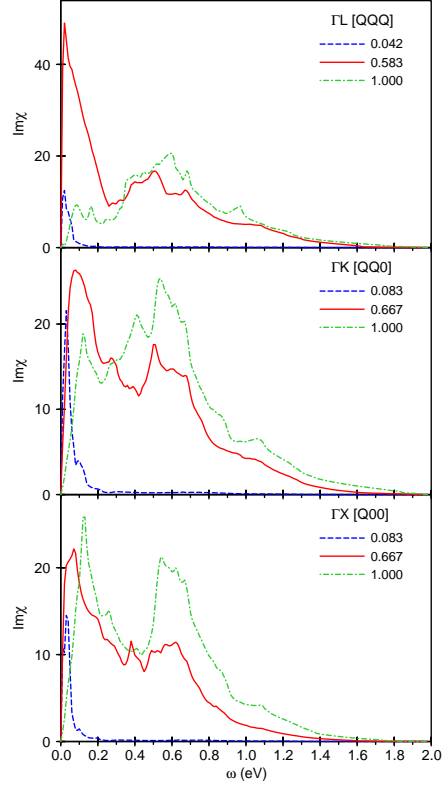


FIG. 5: (Color online) Enhanced  $\text{Im}\chi(\mathbf{Q}, \omega)$  calculated at  $\mathcal{K} = 0.95\mathcal{K}_c$  for the same wavevectors as in Fig. 3. Note: the size along the vertical axis is amplified to that in Fig. 3.

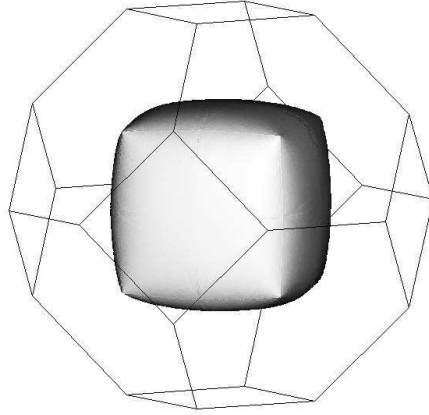


FIG. 6: A surface in  $\mathbf{Q}$ -space representing the lower bound for the “critical” region of strongly enhanced slow spin fluctuations. The upper bound is the larger congruent surface at a distance  $|\delta\mathbf{Q}| \simeq 0.3a^*$  from the smaller one shown.